Book of Tutorials and Abstracts

European Microbeam Analysis Society

EMAS 2023

17th

EUROPEAN WORKSHOP

on

MODERN DEVELOPMENTS AND APPLICATIONS IN MICROBEAM ANALYSIS

7 to 11 May 2023
at the
Jagiellonian University, Auditorium Maximum
Krakow, Poland

Under the auspices of the Rector of the
Jagiellonian University, Krakow, Poland
Organised in collaboration with the
Institute of Metallurgy and Materials Science of
the Polish Academy of Sciences, Krakow, Poland

EMAS
European Microbeam Analysis Society eV
www.microbeamanalysis.eu/

This volume is published by:
European Microbeam Analysis Society eV (EMAS)
EMAS Secretariat
c/o Eidgenössische Technische Hochschule, Institut für Geochemie und Petrologie
Clausiusstrasse 25
8092 Zürich
Switzerland

ISBN 978 90 8227 6961
NUR code: 972 – Materials Science

RECOGNISING AND AVOIDING ION BEAM INDUCED SAMPLE DAMAGE AND ARTEFACTS WHERE IT MATTERS: FIB PROCESSING OF THERMALLY LOW CONDUCTIVE MATERIALS AND FIB EBDS SAMPLE PREPARATION

Annalena Wolff

Caltech, Kavli Nanoscience Institute
1200E California Boulevard, US-91125 Pasadena, CA, U.S.A.
e-mail: awolff@caltech.edu

Annalena (Lena) Wolff obtained her Diploma and PhD degree in Physics in 2014 under the supervision of Professor Andreas Huetten at Bielefeld University before moving to Australia where she worked at the Monash Centre for Electron Microscopy as an electron microscopist. She was recruited to the Queensland University of Technology in 2015 and has established herself as a FIB/SEM and helium ion microscopy (HIM) research infrastructure specialist. Annalena was one of the FIB/HIM/SRIM workshop leaders for AMAS 2017 and IMC 2018. She received an AMAS/EMAS/IUMAS 2017 Early Career Scholarship and is excited to return to EMAS. Since her last EMAS attendance, Lena has taken up a position at the Kavli Nanoscience Institute at Caltech as the resident microscopist, looking after 2 FIB/SEMs, 1 SEM, 1 ESEM, 1 HIM and 1 TEM, supporting ~ 100 users as a sole microscopist. Lena has authored or co-authored 16 papers in internationally recognised and peer reviewed journals, presented 6 invited talks and a keynote lecture on helium ion microscopy.

Annalena Wolff's research interests include: Developing new approaches on SEM/FIB and HIM applications, ion-solid interactions and their simulations, improving FIB/SEM and HIM techniques for biological samples, fabrication of 2D and 3D micro/nanostructures, 3D reconstruction, sample characterisation and analysis including TEM, EDS, EBSD.

1. INTRODUCTION

Focussed ion beams, including Ga or Xe plasma FIB/SEMs, which combine a scanning electron microscope (SEM) and a focussed ion beam (FIB) in a single device, the helium ion microscope (HIM), as well as stand-alone FIB systems, are considered key enabling technology in many research groups and facilities around the globe due to the unique capabilities the system offers. This can be attributed to the vast application range they offer such as nano-fabrication, transmission electron microscopy (TEM) lamella preparation, cross-sectioning, in situ specimen characterisation or 3D-reconstruction with nanometre resolution [1-3]. On the other hand, FIBs (irrespective which instrument is used) induce artefacts that can have deleterious effects on characterisation as well as fabricated device performance [4, 5] and special care needs to be taken when interpreting data generated on FIBs. For example, Ga^+ implantation during the FIB processing of aluminium, leads to Ga accumulation along grain boundaries and changes deformation and fracture behaviour of the material [4]. When creating plasmonic and nano-electronic devices, Ga^+ implantation poisons the devices. In many cases, Ga FIB created artefacts lead to changes and often loss of structure functionality [4-6].

This paper focusses on the ion solid interactions that occur when using FIB systems and looks specifically at recognising and (hopefully) avoiding ion beam induced artefacts with a focus on the lesser reported artefacts of FIB induced heat damage and changes is crystallography which adversely affect EBSD measurements.

This paper reviews the approaches reported in literature to recognise and explain FIB induced heat damage and crystallographic changes that can be deleterious for EBSD measurements and discusses advances in these two fields. A universal approach that can be used by FIB operators in the lab to evaluate deleterious FIB artefacts that requiring a basic understanding of the underlying ion solid interactions combined with Monte Carlo simulations for which the freeware programme SRIM [7] can be used is presented. This approach is demonstrated on two distinctly different topics to show its versatility. The first study, concerning FIB processing of thermally low conductive materials, discusses the physics of ion beam induced heat damage and how to avoid it. The second case study looks at sample altering artefacts that are introduced during FIB processing for electron backscatter diffraction (EBSD).

2. ION-SOLID INTERACTIONS

To gain a better understanding of the ion beam induced sample damage and artefacts it is essential to consider the underlying ion solid interactions that occur, when an energetic ion (irrespective which ion species is used) interacts with a sample. Each incident ion interacts with the sample atoms and loses its energy in a multitude of collisions until it comes to rest (implant) in the sample at a depth called the projected range or alternatively exits the sample. Ions in FIBs interact with the sample atoms in predominantly two ways: Either they interact with the sample

atom's electron cloud (inelastic collisions), or they interact with the sample atom's nucleus (elastic interactions). Throughout these interactions, the ions lose their energy $\frac{dE}{dx} = \frac{\mathrm{d}E_{\mathrm{el}}}{dx} + \frac{\mathrm{d}E_{\mathrm{nucl}}}{dx}$.

These two types of interaction give rise to all possible interaction types illustrated in Fig. 1. The collisions can lead to sputtering of sample surface atoms, sample atom displacements such as vacancies, a collision cascade and replacement collisions, phonons, as well as backscattered ions. Secondary electron and secondary ion emission as well as polymerisation are additionally caused by the ion-solid interactions. If a sufficiently high number of sample atoms are displaced from their initial sample position, amorphisation occurs. The loss of crystallinity can be seen in the HRTEM image of Si in Figure 2. Heat is generated in the different interaction types that occur during this process: Electronic excitation and relaxation, emission and recapturing of electrons and photons, as well as direct energy losses to phonons in nuclear collisions [8]. A detailed discussion on ion solid interactions can be found in [4, 9]. Figure 1 shows the statistics for He, Ne, Ga when interacting with a Si sample. Here 10,000 ions were simulated using SRIM and the secondary electron emission, vacancy production, sputtered atoms and backscattered ions determined. The statistics show that significantly more vacancies (a factor of several hundred to several thousand times, depending on ion species and chosen FIB parameters) are created than atoms sputtered. This is expected to lead to significant artefacts when processing samples using FIB and a thorough understanding and evaluation of which artefacts occur where in the sample is essential to avoid problems with subsequent analysis (or device performance for that matter). Whether, or how much, a specific artefact will adversely affect a measurement or device performance needs to be evaluated for each case individually. A flexible, yet universally applicable approach to assess FIB damage is thus important.

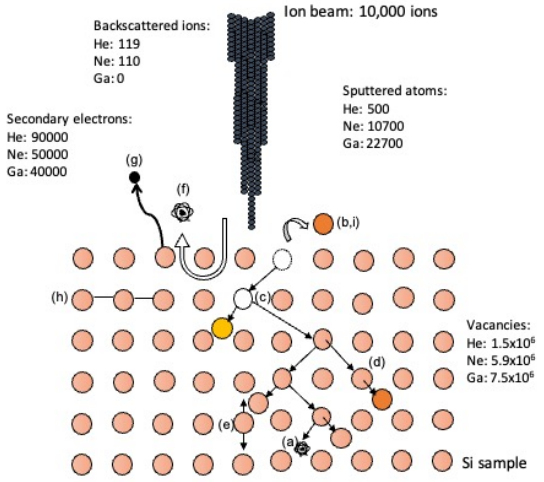

Figure 1. Illustration of the ion solid interactions and their statistics for He, Ne, Ga ions. A multitude of interactions result from the inelastic and elastic collisions: a) ion implantation, b) sputtering, c) sample atom displacements incl. vacancies, d) collision cascades and replacement collisions, e) phonons, f) backscattered ions, g) secondary electron (SE) emission, h) polymerisation, and i) secondary ion emission. SRIM simulations were used to determine the number of vacancies, SE emission, backscattered ions as well as sputtered sample atoms.

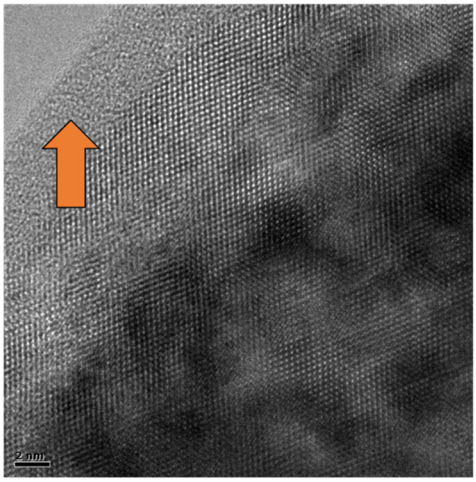

Figure 2. HRTEM image of Si, recorded using a Tecnai TF30 at 300 kV. The FIB induced amorphous layer can easily be recognised on the left hand side and is indicated by the orange arrow. The amorphous layer resulted in this place during the TEM lamella thinning polishing process. The thickness of the lamella is thinner than the FIB induced amorphous layers, leading to complete sample amorphisation in this area.

3. *FIB PROCESSING OF THERMALLY LOW CONDUCTIVE MATERIALS*

Throughout the past decades, FIB work focussed predominantly on thermally conductive and hard materials such as Si and metals. For Si, the temperature increases less than 2 °C [8], which has often lead to heating effects being neglected. Today, however, FIB/SEMs are increasingly used to prepare thermally low conductive materials [10], for example polymers or biological samples. Several studies have explored heat damage and have offered sets of parameters, which achieved acceptable results for the specific [5, 6, 11]. However, a universally applicable and adaptive FIB processing approach has only recently been proposed [8]. The physical model proposed in that work is based on Fourier's law of conductive heat transfer $\overline{q} = -k\nabla T$ with $\overline{q}$ as the local heat flux density [W/m^2], k as the thermal conductivity [W/mK], and ∇T T as the temperature gradient [K/m]. In their work Wolff *et al.* [8] adapted Fourier's law to

$$\Delta T[\mathrm{K}] = \frac{(\Delta E_{\mathrm{el}}[\mathrm{J}] + \Delta E_{\mathrm{phonon}}[\mathrm{J}])^{*}\mathrm{N}}{t\,[\mathrm{s}]*A[\mathrm{m}^2]} * \frac{R_{\mathrm{proj}}[\mathrm{m}]}{k\left[\frac{\mathrm{W}}{\mathrm{mK}}\right]}$$

which highlights the FIB parameters more directly. The model describes the locally induced heat for a single scan point. A detailed description of the adapted model can be found here [8]. Being able to directly visualise which parameters induce heat damage allows the operator to find more suitable FIB setting to process a thermally low conductive material and to avoid FIB induced heat damage.

Throughout FIB processing, each ion loses a specific amount of energy to phonons ΔE_{phonon} and in inelastic collisions ΔE_{el} , per dwell time t, leading to changes in sample temperature. The actual energy losses per ion ΔE_{el} and E_{phonon} can be determined in Monte Carlo simulations using the freeware programme SRIM [7]. Here the specific ion species, energy and incidence angle need to be specified as well as the sample material. All other parameters that are required to determine the FIB induced change in sample temperature are instrument parameters such as the dwell time t, number of ions N and ion beam diameter for specific conditions (A) that can be set during operations. A qualitative evaluation of the proposed model suggests that ion beam induced heat can be minimised by lowering the heat flux either via reducing the ion beam current (reduced N) and by increasing the area on the sample with which the energetic ions interact (A) or potentially via lowering the actual energy losses to phonons and electronic energy losses (ion energy) or a combination of those parameters. Wolff *et al.* [8] showed that a combination of parameters (significantly reduced beam current, beam blur and increased overlap) significantly lowered the ion beam induced changes in temperature that allowed to process collagen. Purified collagen (principle component of skin) is an excellent test material to study FIB induced heat damage since literature values are readily available and because heat denaturated collagen loses its fibrillary structure [26], which is recognisable using microscopy techniques.

SRIM results for 30 keV Ga^+-ions interacting with collagen show that the ions lose the majority of their initial energy (~ 90 %) to phonons and ionisation, both of which induce heat in the sample. As a result, severe heat damage results when processing the thermally low conductive material using conventional FIB parameters (30 keV ions and nA beam current), with sample temperatures estimated to reach ~ 2,500 °C [8] for collagen/skin, which has a thermal conductivity $k = 0.29$ [W/(m·K)]. Whilst reducing the beam current slightly and blurring out the beam several hundred nanometres reduces the ion beam induced temperature change, the achieved temperature difference for a 1 nA beam current, 20 % beam overlap and a 200 nm blur can be calculated to 114 °C, which is still above the reported degradation temperature for collagen at 65 °C [25]. This suggests that adjusting a single parameter such as the ion interaction area A is insufficient to achieve the required reduction in FIB induced sample temperature changes. In general, a change in several parameters may be required, especially for lower thermally conductive materials. The evaluation suggests nA ion beam currents cannot be used to process this specific thermally low conductive material when using 30 keV Ga^+-ions to process collagen. Indeed, lower pA beam currents in combination with beam blur were required when processing with 30 keV Ga^+-ions to avoid FIB induced heat damage [8]. Medium range currents around 0.1 nA were reported to induce temperature changes up to 1,233 °C [8]. Smaller FIB currents have a smaller beam diameter and this leads to a non-linear decrease in induced temperature by lowering the beam current, making it hard to estimate a suitable ion beam current as the changes in beam diameter need to be additionally considered. Whilst the overall approach was successful for collagen/skin it is expected that the reduction in beam current and increase in beam diameter may not be sufficient for materials with thermal conductivities $k < 0.29$ [W/(m·K)] as significant further reduction in ion beam current is not possible for cutting cross-sections. A thorough look at the previously proposed model suggests that the heat flux

could also be reduced by changing the ion energy. The SRIM simulations for 5 keV Ga^+-ions impacting collagen/skin show that the ions also lose over 90 % to phonons and ionisation. The total amount of energy losses to ionisation and phonons per ion was determined to 4.7 keV and is significantly lower than 28.8 keV for 30 keV Ga^+-ions. The estimated temperature change when using 5 keV ion energy and a mid-range ion beam current of 0.12 nA without requiring a blur can be determined using the model to 4.5 °C. This is a significant reduction in FIB induced temperature changes and is well below the reported degradation temperature for collagen. This approach could allow processing of materials with thermal conductivities $k < 0.29$ [W/(m·K)] in general as further reduction in ion beam current is possible and beam blur can still be added.

The obtained theoretical results were experimentally tested by FIB processing collagen with 30 keV and 5 keV ions and assessing any potential ion beam induced heat by evaluating the loss of fibrillary structure in SEM and TEM measurements. The resulting unnaturally smooth surface areas, visible in the SEM image in Figs. 3a and 3b when using accelerating voltage of 30 kV and mid range 0.1 nA - 1 nA beam currents indicates the ion beam induced heat damage. The heat damage is not visible when using a reduced ion energy to 5 keV (Fig. 1c) despite using mid range ion beam currents of 0.12 nA. The results also match the predicted outcomes using the model proposed earlier by Wolff *et al.* [8]. The TEM analysis (Fig. 4) of FIB prepared TEM lamella using 30 keV ions (Fig. 4a) as well as using the 5 keV lower ion energy approach (Fig. 4b), both with nA beam currents for cross-sectioning and elevated ion beam currents (0.5 nA for 30 keV; 0.6 nA for 5 keV) for coarse thinning, (0.1 nA for 30 keV; 0.23 nA for 5 keV) for thinning show that the native collagen structure could be maintained when using the low ion energy approach despite using elevated ion beam currents throughout the entire process. A collapsed/denaturated structure was found for the 30 keV ion energy when using elevated ion beam currents. Wolff *et al.* [8] suggested that significantly lower ion beam currents (lower pA range) need to be used for TEM lamella preparation when working with collagen.

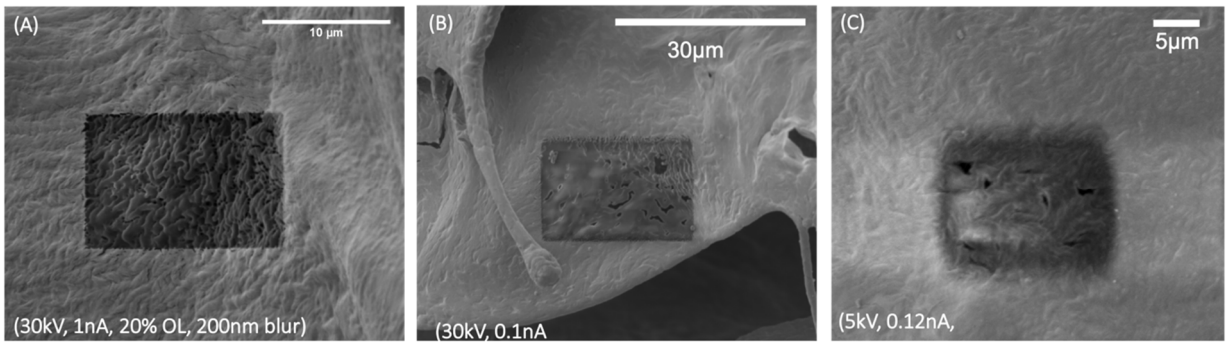

Figure 3. SEM images of FIB processed collagen using different ion beam parameters. a) High ion energy (30 keV) FIB processing with nA beam currents leads to heat damage which can be recognised as unnaturally smooth areas within the FIB processed area. b) High ion energy (30 keV) FIB processing with a mid-range beam current of 0.1 nA shows significant heat damage. c) Low ion energy (5 kV) FIB processing with mid-range beam currents allows maintaining the natural collagen structure.

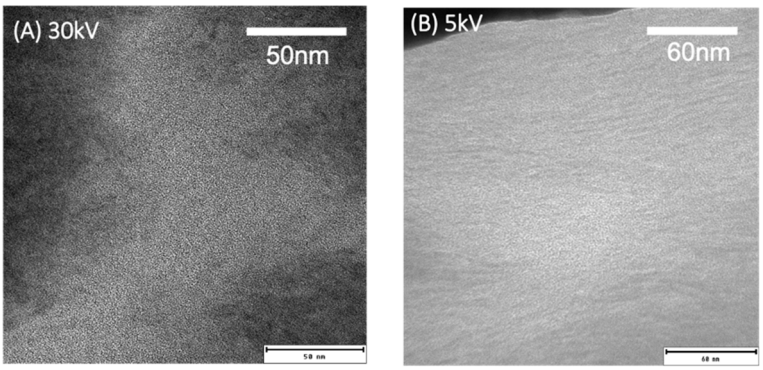

Figure 4. TEM measurements of collagen prepared with a) 30 keV ions, and b) 5 keV ions. Collagen's fibrillary structure can only be observed for the low ion energy processing.

The work shows how combining a basic understanding of physics and ion solid interactions with Monte Carlo simulations allows to select meaningful FIB parameters from a multitude of possibilities prior to an experiment. Heat damage to the thermally low conductive material could be avoided this way. This approach opens up FIB processing for a wider class of materials such as polymers or biological samples in a safe manner: suitable parameters can be estimated and tried prior to the experimental session, reducing both the risk of sample/instrument damage as well as saving time in the lab.

4. FIB POLISHING FOR EBSD EXPERIMENTS: OUTRUNNING THE FIB INDUCED DAMAGE

EBSD, allowing to study microstructure, grain size, and orientation, as well as strain of a crystallographic sample, in addition to allowing phase analysis, is considered a standard characterisation technique in microscopy today [12, 13]. Different polishing approaches have been used over the years [14-17] and FIBs are a now frequently used in EBSD sample preparation to achieve the required mirror-flat sample surface [19, 20]. Whilst FIB damage is recognised in this field [20-23], artefacts in EBSD sample preparation are often not published. This part of the manuscript aims to show that the proposed approach to use SRIM simulations and an evaluation of the ion solid interactions, specifically calculating the ion implantation concentration as well as vacancy formation analysis, can be used to explain artefacts and most importantly to select appropriate FIB systems and parameters to allow a meaningful EBSD analysis.

Previous work by J. Michael [20, 21] reported that Ga FIB processing induces phase transformations of Cu to Cu_3Ga as well as microtextural modifications. An SEM image of the described phase transformations is shown in Fig. 5. The recent study by Wolff [24] showed that these phase transformations occur in areas of the sample where a sufficiently high impurity concentration of implanted Ga^+-ions is achieved, during the polishing process, irrespective if a high ion energy (30 keV) or a low energy (2 keV) glancing angle approach is used. The phase

transformations, verified by TEM selected area electron diffraction (SAED) as well as EBSD phase analysis are shown in Figs. 5a to 5d. The non-homogeneous distribution of phase-transformed areas can be understood when taking both ion implantation and the channelling artefact into account. Whether or not a phase transformation occurs depends on the implanted concentration of Ga ions that result in the FIB process. This impurity concentration is limited by the steady state condition when working with FIBs that are optimised for milling [24] as ions which were previously implanted are removed in the sputtering process and new ions implanted, effects that will eventually balance out. The steady state condition is reached once a sample has been milled down to the interaction volume depth. To determine this parameter SRIM simulations are used to estimate the interaction volume depth. For 30 keV Ga^+-ions impacting copper at a 0° incidence angle, the interaction volume depth ~ 25 nm is close to the EBSD signal depth. The time it takes to reach the steady state condition is the determined experimentally by milling a rectangle with a set time. The actually milled depth is the determined using either SEM or TEM (TEM lamella preparation is required here but will provide more accurate results). The time until the steady state condition can then be calculated via

$$T_{steady\text{-}state}[s] = {milling\ time[s]}/{measured\ milled\ depth\ [nm]} \times \text{interaction volume depth [nm]}.$$

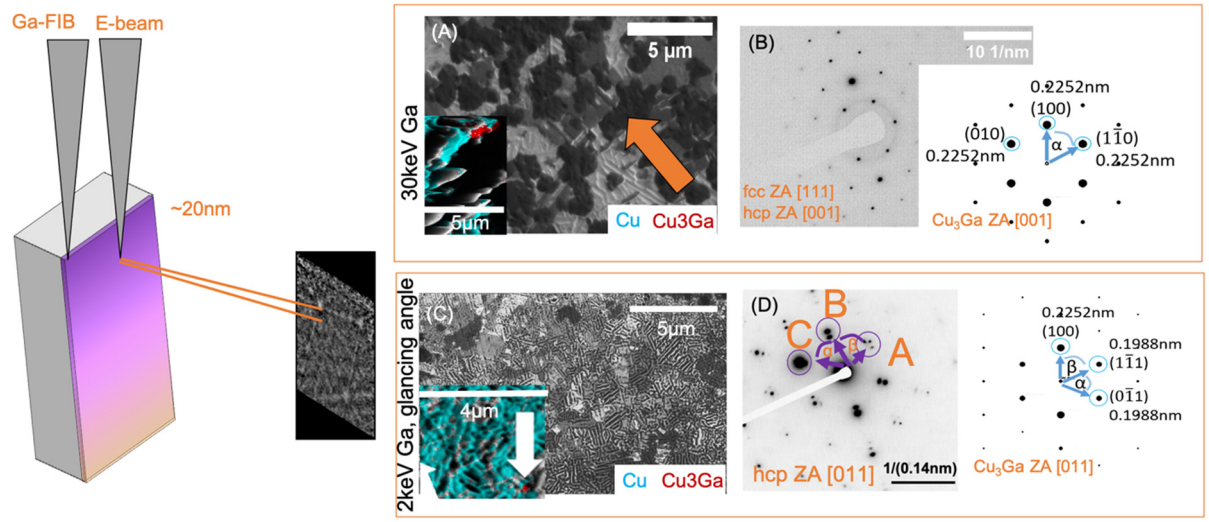

Figure 5. FIB, TEM, SAED and EBSD measurements showing the resulting phases after polishing a Cu sample with different ion species and FIB parameters. a) FIB image showing darker regions where Cu transformed into Cu_3Ga during 30 keV Ga^+-irradiation. The EBSD phase map of the corresponding region is shown in the inset. b) SAED measurements and the corresponding simulation and evaluation show that the crystal structure of the sample corresponds to a Cu_3Ga phase. c) FIB image showing darker regions where Cu transformed into Cu_3Ga during 2 keV Ga^+-irradiation at glancing angles. The EBSD phase map of the corresponding region is shown in the inset. d) SAED measurements and the corresponding simulation and evaluation show that the crystal structure of the sample corresponds to a Cu_3Ga phase.

The published work by Wolff [24] showed that the different grains mill differently fast within the same processing time and thus reach the steady state condition at different times. As a result, slow milling grains can reach a higher Ga impurity concentration while fast milling grains accumulate less Ga^+-ions. The number of implanted ions for the used ion beam current can be calculated for each steady state condition using the following approach:

$$N = \frac{I_{Ion}\,[A] \times t\,[s]}{charge\,[C]}$$

with N as the number of implanted Ga^+-ions, t as time it takes to reach the steady state condition and using the elementary charge and the used ion beam current I_{Ion}. This is an estimate only as sputtering and backscattered ions are not considered. The calculation thus presents an upper limit. Wolff [24] determined the number of implanted ions for slow milling grains to (7.6×10^{10} Ga^+-ions and 3.8×10^{10} Ga^+-ions for fast milling grains [24]. The impurity concentration can then be determined when considering the number of sample atoms that exist within the interaction volume. Wolff [24] showed that Ga impurity concentrations between 18 % for fast milling grains (insufficient for a phase transformation to Cu_3Ga) and up to 36 % for slow milling grains (sufficiently high for a phase transformation to Cu_3Ga) occur during FIB processing with 30 keV Ga^+-ions. This explains why the phase transformations only occur in specific regions on the sample initially: A sufficiently high impurity concentration is reached in the slow milling grains but not in the fast milling grains. To avoid phase transformations either a different, inert, ion species can be used for FIB polishing such as Ne or conditions must be found, which allow to achieve the steady state condition fast to limit the FIB induced Ga impurity concentration below the threshold for phase transformations. The results published by Wolff [24] show that phase transformations could not be avoided even when using the commonly employed approach of low energy glancing angle irradiations, suggesting that Ga FIBs are not suitable to polish Cu for EBSD measurements. Polishing with 25 keV Ne^+-ions, however, avoided phase transformations and improved indexing quality of the EBSD maps. The TEM and EBSD measurements for 25 keV Ne^+-polishing at glancing angles are shown in Fig. 6.

Both Michael [21] and Wolff [24] showed that significant crystallographic changes can occur during FIB processing. Wolff showed significant changes in high angle grain boundaries (HAGB) and low angle grain boundaries (LAGB) as well as altered Kernel average misorientation maps (KAM) can easily occur and prevent a meaningful stress and strain analysis. This artefact occurred irrespective of ion species (Ga and Ne) but could be linked to the resulting vacancy formation with in the sample during FIB processing [24]. A comparison of the LAGB and HAGB for the different polishing conditions (Table 1) against an unpolished control experiment reported by Wolff [24] shows the changes in stress/strain for different FIB parameters. Changes in HAGB and LAGB could be avoided when polishing with 25 keV Ne^+-ions at glancing angle only. The corresponding KAM map for that measurement and the control experiment (unpolished Cu) is shown in Fig. 6. Why using a glancing angle incidence angle was required to avoid changes in crystallography was required can be understood when considering the number of vacancies that are created for the different FIB settings.

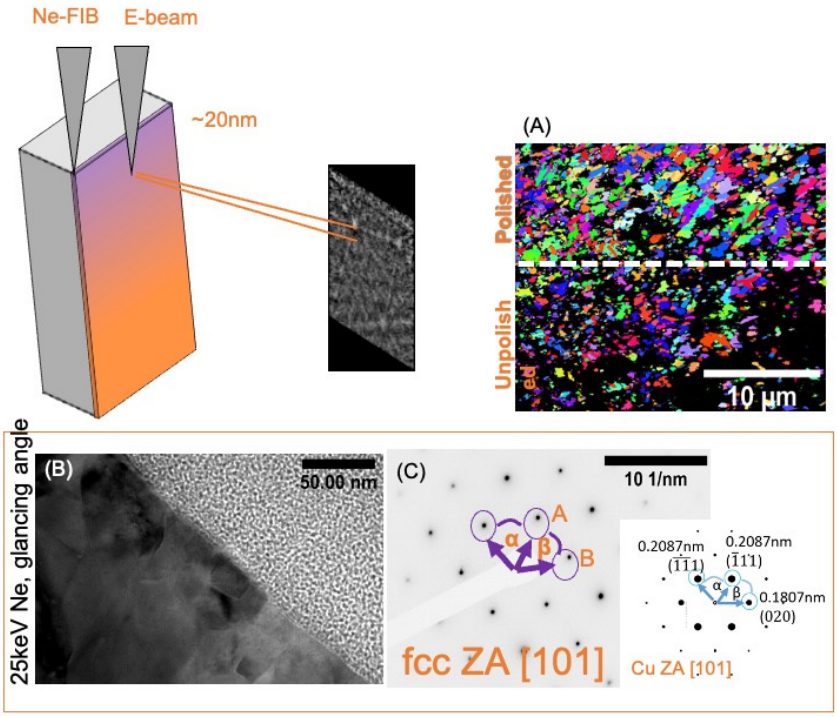

Figure 6. TEM, SAED and EBSD measurements showing the results of polishing Cu with 25 keV Ne^+ at glancing angles. a) EBSD measurements showing the IPF orientation map of the polished and unpolished Cu sample. b) TEM image showing the cross-section of the Ne-polished Cu sample. c) SAED measurement and the corresponding simulation show that the crystal structure of the sample corresponds to the original Cu phase.

Table 1. LAGB and HAGB for various FIB polishing conditions, reported by Wolff [26].

	Control experiment	30 keV Ga	2 keV Ga glancing angle	25 keV Ne glancing angle
HAGB %	92	56	83	92
LAGB %	8	44	17	8

SRIM can be used to estimate the number of vacancies that are created during the FIB process. The vacancy plot for 25 keV Ne glancing angle irradiation is shown in Fig. 7. It is important to consider the vacancies here instead of the displacements. A displacement can either be a vacancy or a replacement collisions and later replaces the sample atom with another identical sample atom. The plots for 25 keV Ne at glancing angle shows that 176 Vacancies / Å-ion are created. Converting this value to Vacancies / Å-cm and multiplying it with the ion dose at which the steady state condition is reached gives the number of vacancies that are created per volume:

$$\text{Vacancies / Å-cm} \times \text{ion dose (ions/cm}^2\text{)} = \text{vacancies /cm}^3$$

with the dose as

$$N\backslash A = \frac{I_{Ion}\,[A] \times t\,[s]}{\text{charge}\,[C]\;A}$$

with N as the number of ions, t as time it takes to reach the steady state condition and A as the irradiated/polished area. A comparison to the atomic density then reveals how many atoms are displaced or, if sufficiently high, how often each atom was displaced. Wolff [24] reported that each atom was displaced up to 138 times when using 30 kV Ga, 22 times when polishing with 2 keV Ga at glancing angle, and up to 266 times when using 25 keV Ne in a frontal polishing approach. The lowest number of displacements (17 times) was achieved when polishing with Ne at glancing angles. The number of displacements was found to directly correspond to the degree of change in LAGB/HAGB.

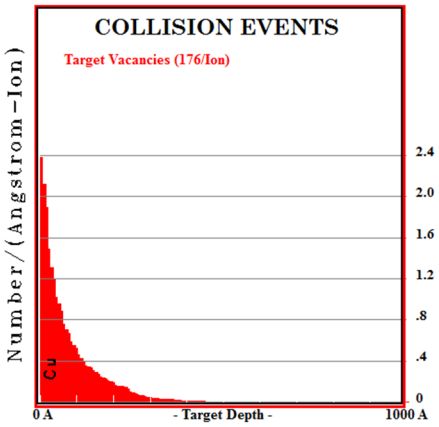

Figure 7. Vacancies SRIM plot for 25 keV Ne^{+}-ions hitting a Cu sample at glancing angles.

By using SRIM to calculate both the implanted ion impurity concentration as well as the number of vacancies created, the underlying causes for the local phase transformation and crystallographic changes to a sample could be explained. Suitable FIB parameters and ion species could be determined to successfully prepare EBSD samples. Using 25 keV Ne^{+}-ions at glancing angle, phase transformations can be avoided as a result of using an inert ion species. The crystallographic changes could also be avoided as the parameters outrun the FIB induced damage by allowing to reach the steady state condition fast and thus limiting the vacancy formation that causes stress/strain.

5. METHODS FIB PROCESSING OF THERMALLY LOW CONDUCTIVE MATERIALS

SRIM was used to model the ion solid interactions of 30 keV Ga^+-ions as well as 5 keV Ga^+-ions. 50,000 ions were simulated for each of the conditions. To ensure accuracy the 'surface sputtering/monolayer collision step' was selected as calculation type and the window size chosen in such a way that all ion trajectories could be followed to the end.

The FIB cross-sections as well as the TEM lamellae were prepared using a FEI Quanta 200 3D. The SEM images were recorded using the same system using 5 kV acceleration voltage and 90 pA beam current, 1 µs dwell time, 128 frames integration filter and 1,024 × 882 pixel resolution with an Everhart-Thornley detector. The TEM lamella were analysed using a JEOL 2100, operated at 200 kV. All experiments were performed at the Central Analytical Research Facility operated by the Queensland University of Technology, Brisbane, Australia.

A detailed description of the methods, including collagen sample preparation can be found in [8].

6. METHODS FIB POLISHING FOR EBSD EXPERIMENTS: OUTRUNNING THE FIB INDUCED DAMAGE

Different FIB systems, a Thermo Scientific Scios (Ga) FIB/SEM as well as the Zeiss helium ion microscope (Ne) were used to irradiate conventional copper TEM grids at different glancing angles and ion energies using a dose of 2,247 - 3,371 ions/nm^2. The subsequent EBSD analysis of the bulk samples was carried out using an Oxford Symmetry EBSD detector on a TESCAN S8000X Xe plasma FIB/SEM. The TEM lamella were prepared from the bulk using standard techniques on the Scios (Ga) FIB/SEM. The TEM analysis was performed on a JEOL 2100 operating at 200 kV. The Ga^+-irradiation experiment and TEM lamella preparation were performed at the Centre for Microscopy and Microanalysis, operated by the University of Queensland. All other experiments, were performed at the Central Analytical Research Facility operated by the Queensland University of Technology, Brisbane, Australia.

SRIM was used to model the ion solid interactions for different experiments. To ensure accuracy the 'surface sputtering/monolayer collision step' was selected as calculation type and the window size chosen in such a way that all ion trajectories could be followed to the end.

A detailed description of the sample preparation for can be found in [24].

7. CONCLUSION

Using the underlying ion solid interactions in FIB and using SRIM to simulate the corresponding experiments is a powerful combination to explain, understand and avoid deleterious FIB induced sample alterations (where possible). Two distinctly different examples across different research fields were reviewed that focus on lesser discussed FIB artefacts: (1) FIB induced heat damage when processing thermally low conductive materials; and (2) phase transformations and crystallographic changes resulting from FIB processing for EBSD measurements.

In both case studies, the approach of using SRIM and evaluating the ion solid interactions allowed to explain and then avoid FIB induced artefacts, making it a universal and powerful approach for FIB operators.

8. ACKNOWLEDGEMENTS

The author gratefully acknowledges the contributions and work of the co-authors Dr Nico Klingner, Dr William Thompson, Dr Yinghong Zhou, Dr Jinying Lin, Prof Yin Xiao , Ms Yong Y. Peng and Dr John A.M. Ramshaw for providing the collagen samples, COMSOL simulations and numerical modelling concerning the work presented and referenced in the section FIB processing of thermally low conductive materials. This work could not have been carried out (and published) without this team.

With respect to the second presented topic on FIB for EBSD sample preparation, the author would like to sincerely thank Dr Peter Hines, Dr Jamie Riches, and Dr Graeme Auchterlonie for the discussions about the TEM results and crystallography. The author would like to thank Dr Jamie Riches for the support on the TEM and for preparing the sample using PIPS. The author would like to thank Prof Nikki Stanford and Dr Vijay Bhatia for the discussions about EBSD. The author would like to thank Rebecca Fieth for preparing the electropolishing samples.

The author acknowledges the Central Analytical Research Facility at the Queensland University of Technology where most of the work was conducted on the either of the following systems: Zeiss Orion Nanofab (HIM), JEOL 2100 (TEM), TESCAN S8000X (PFIB/SEM), FEI Quanta 3D (Ga FIB/SEM). The author would also like to acknowledge the Centre for Microscopy and Microanalysis operated by the University of Queensland for the access to the Thermo Scientific Scios Ga FIB/SEM. The author would like to thank the authors of the programs SRIM and FIJI for making the software freely available.

9. REFERENCES

[1] Young R J, Moore M V 2005 Dual-beam (FIB-SEM) systems. in: *Introduction to focused ion beams*. (Giannuzzi L A and Stevie F A; Eds.) [New York, NY: Springer]

[2] Drobne D, Milani M, Leser V and Tatti F 2007 *Microsc. Res. Tech.* **70** 895-903

[3] Orloff J, Utlaut M and Swanson L 2003 *High resolution focused ion beams, FIB and it's applications*. [Amsterdam, The Netherlands: Kluwer Academic / Plenum Publishers]

[4] Einsle J, Bouillard J, Dickson W and Zayats A V 2011 *Nanoscale Res. Lett.* **6** 572

[5] Xiao Y, Maier-Kiener V, Michler J, Spolenak R and Wheeler J M 2019 *Mater. Design* **181** 107914

[6] Bassim N D, de Gregorio B T, Kilcoyne A L D, Scott K, Chou T, Wirick S, Cody G and Stroud R M 2011 *J. Microscopy* **245** 288-301

[7] Ziegler J F, Biersack J P and Ziegler M D 2015 *SRIM – the stopping and range of ions in matter*. [Morrisville, NC: Lulu Press Co.]

[8] Wolff A, Klingner N, Thompson W, Zhou Y, Lin J, Peng Y, Ramshaw J and Xiao Y 2018 *J. Microscopy* **272** 47-59

[9] Giannuzzi L A and Stevie F A 2005 *Introduction to focused ion beams*. [New York, NY: Springer]

[10] Villinger C, Gregorius H, Kranz C, Hoehn K, Muenzberg C, von Wichert G, Mizaikoff B, Wanner G and Walther P 2012 *Histochem. Cell. Biol.* **138** 549-556

[11] Diez-Escudero A, Espanol M, Montufar E B, Di Pompo G, Ciapetti G, Baldini N and Ginebra M 2017 *Tissue Eng. C: Methods* **23** 118-124

[12] Wilkinson A J and Britton T B 2012 *Mater. Today* **15** 366-376

[13] Schwartz A J, Kumar M and Adams B L (Eds.) 2000 *Electron backscatter diffraction in Materials Science*. [Newx York, NY: Springer]

[14] Nowell M M, Witt R A and True B 2005 *Microsc. Microanal.* **11** 504-505

[15] Wynick G L and Boehlert C J 2005 *Mater. Charact.* **55** 190-202

[16]

[17] Kim D I, Kim B K and Kim J H 2015 *Appl. Microsc.* **45** 218-224

[18] Saowadee N, Agersted K, Ubhi H S and Bowen J R 2013 *J. Microscopy* **249** 36-40

[19] Michael J R and Giannuzzi L 2007 *Microsc. Microanal.* **13** 926-927

[20] Michael J R 2006 *Microsc. Microanal.* **12** 1248-1249

[21] Michael J R 2011 *Microsc. Microanal.* **17** 386-397

[22] Xiao Y, Maier-Kiener V, Michler J, Spolenak R and Wheeler J M 2019 *Mater. Design* **181** 107914

[23] Kiener D, Motz C, Rester M, Jenko M and Dehm G 2007 *Mater. Sci. Eng. A* **459** 262-272

[24] Wolff A 2021 *Beilstein J. Nanotechnol.* **12** 965-983

[25] Bozec L and Odlyha M 2011 *Biophysical J.* **101** 228-236

[26] Zeugolis D I, Khew S T, Yew E S, Ekaputra A K, Tong Y W, Yung L Y, Hutmacher D W, Sheppard C and Raghunath M 2008 *Biomaterials* **29** 2293-2305